



OPEN

Profiling individual human red blood cells using common-path diffraction optical tomography

SUBJECT AREAS:
BIOLOGICAL PHYSICS
HAEMATOLOGICAL DISEASES
CELLULAR IMAGING

Received
24 June 2014

Accepted
29 September 2014

Published
17 October 2014

Correspondence and requests for materials should be addressed to
S.J. (ssjang@amc.seoul.kr) or Y.K. (yk.park@kaist.ac.kr)

* These authors contributed equally to this work.

† Current address:
Photonics Group,
Department of Physics,
Imperial College
London, London SW7
2AZ, United Kingdom.

‡ Current address:
Seegene Medical Foundation, Seoul
133-847, Republic of Korea.

¹Department of Physics, Korea Advanced Institute of Science and Technology, Daejeon 305-701, Republic of Korea,

²Department of Laboratory Medicine, University of Ulsan, College of Medicine and Asan Medical Center, Seoul 138-736, Republic of Korea.

Due to its strong correlation with the pathophysiology of many diseases, information about human red blood cells (RBCs) has a crucial function in hematology. Therefore, measuring and understanding the morphological, chemical, and mechanical properties of individual RBCs is a key to understanding the pathophysiology of a number of diseases in hematology, as well as to opening up new possibilities for diagnosing diseases in their early stages. In this study, we present the simultaneous and quantitative measurement of the morphological, chemical, and mechanical parameters of individual RBCs employing optical holographic microtomography. In addition, it is demonstrated that the correlation analyses of these RBC parameters provide unique information for distinguishing and understanding diseases.

The morphological, chemical, and mechanical parameters of red blood cells (RBCs) have strong correlations with the pathophysiology of many diseases¹. Optical microscopy has been widely used to image the shapes of RBCs in blood smears in order to evaluate poikilocytosis (e.g. spherocytes, target cells) and blood-borne infectious diseases including malaria. The chemical information about RBCs, and particularly about cytoplasmic hemoglobin (Hb), which are described using parameters such as mean corpuscular Hb concentration (MCHC) and mean corpuscular Hb content (MCH), are being used for medical diagnosis on a daily basis in laboratory medicine. Recent research has demonstrated that measuring the mechanical properties of RBCs enables the probing of subtle alterations in the membrane structures of RBCs that can result from several infectious diseases and genetic disorders (e.g. malaria and sickle cell disease)^{2–4}. In order to analyze the properties of RBCs, automated blood cell counters based on the complete blood count (CBC) have been most commonly used in clinical hematology⁵. In a routine blood examination using CBCs, several red cell indices, including MCH, MCHC, mean corpuscular volume (MCV), and RBC distribution width (RDW), are obtained. These indices from the CBC serve as the primary and critical information from which clinicians diagnose abnormalities in RBCs. However, in abnormal pathological conditions, limitations exist for making accurate hematological diagnoses. This results from the current automated blood cell counter techniques only measuring limited number of parameters on RBCs, including MCV, MCHC, MCH, and RDW.

Because the regulation of the dynamic systems of RBCs and their related pathophysiology is understood using detailed analyses of individual cells⁶, a single-cell profiling technique for RBCs may hold the key to the understanding, diagnosis, and prognosis of many blood-related diseases with applications ranging from basic science to clinical practices. Currently, very few approaches to single cell profiling have been explored^{7–11}. However, the existing techniques cannot provide the complete characterization of individual RBCs. For example, the Hb content of RBCs is typically calculated from hematocrit after hemolysis in an averaged manner. The volumes of individual RBCs can be obtained with impedance¹² or light scattering measurements¹³, but these methods depend on certain assumptions or require additional treatment including spherling agents. The cell surface area and sphericity have been addressed using indirect methods such as osmotic feasibility tests or flow-based imaging techniques, which are subject to low precision and technical limitations^{14,15}. Recently, quantitative phase-imaging (QPI) techniques have been used to characterize RBCs at the individual cell level^{16–22}; for example, tomographic phase microscopy measures the structural and chemical information (e.g. cell volume, Hb concentration, and Hb content) of RBCs². In particular, the mechanical properties of individual RBCs have been investigated through probing the dynamic membrane fluctuations in cell membranes using QPI techniques^{18,23–25}. These methods have significantly enhanced the understanding of RBCs; yet none of the existing techniques simultaneously and



comprehensively measure the complete parameters of RBCs at the individual cell level. Despite the strong motivation for single cell profiling, it is technically challenging to achieve complete characterizations of individual RBCs.

In this paper, the morphological, chemical, and mechanical parameters of individual RBCs are simultaneously characterized employing common-path diffraction optical tomography (cDOT), non-invasive and label-free laser holographic microscopy. Single cell profiling of RBCs was performed in four different pathophysiological groups: RBCs from a healthy individual, RBCs from a patient with iron deficiency anemia (IDA), reticulocytes from a patient with a high reticulocyte content, and RBCs from a patient diagnosed with hereditary spherocytosis (HS). The morphological, chemical, and mechanical parameters of the RBCs within these groups were quantified at the individual cell level. The present technique presents many potential advantages over current clinical hematology analyzers in that it can measure the surface area, sphericity, and mechanical properties of individual RBCs which the current hematology analyzers cannot measure, in addition to MCV, MCHC, MCH, and RDW without requiring spherification of cells. Moreover, it is demonstrated that the correlation analyses between the RBC parameters from these patients enabled the investigation of the related pathophysiology in detail and also demonstrated distinct deviations from the distributions of the RBCs from healthy subjects.

Results and Discussions

Common-path diffraction optical tomography (cDOT). For simultaneous measurements of the morphological, chemical, and mechanical parameters of individual RBCs, we employ cDOT, a recently developed optical technique which allows simultaneous measurements of the 3D refractive index (RI) tomography and dynamic 2D membrane fluctuations of individual samples.

The experimental scheme of cDOT is based on the principle of common-path laser-interferometric microscopy and optical diffraction tomography²⁶ (Fig. 1A). A sample is positioned between two objective lenses, and then illuminated by a plane-wave laser beam with specific angles of illumination. The angle of the beam illuminating the sample is precisely scanned by a two-axis galvanometer mirror (GM1). GM2, located at the conjugated plane to the sample and GM1, is synchronized with GM1 in order to de-scan; the angle of the beam reflected from GM2 remains unchanged regardless of the illumination angle. A spatially modulated hologram of a sample is recorded onto an image sensor from which the optical field of the diffracted beam from the sample, containing both amplitude and phase information, can be retrieved using a phase retrieval algorithm²⁷. The details of the method can be found elsewhere^{26,28,29}.

The synchronization between angle-scanning by GM1 and angle-descanning by GM2 is precisely adjusted to work together, which allows simultaneous measurements of the 3D RI tomography and dynamic 2D membrane fluctuations of individual samples (Fig. 1A inset).

By varying the angles of the illumination beam, cDOT measures multiple 2D optical fields, from which 3D RI tomograms of the sample are reconstructed using an optical diffraction tomography algorithm^{30,31}. For the measurements of the RBC mechanical properties, the angle of the illumination beam is fixed to be normal to the sample and dynamic 2D optical-field images are measured, from which the dynamic membrane fluctuations of the cell can be quantified.

From these measured 3D RI tomograms and 2D dynamic membrane fluctuations of individual RBCs, the volume, surface area, sphericity, Hb content, and Hb concentration can be obtained at the single cell level, as summarized in Fig. 1B. The 3D RI of RBCs can be directly and quantitatively translated into the Hb concentration because the RBC cytoplasm primarily consists of Hb protein. Thus, the Hb content and concentration values of the individual

RBCs can be calculated using the 3D RI tomograms. At the same time, cDOT measures the dynamic membrane fluctuations of RBCs, which manifest their mechanical properties. Furthermore, the correlation between these properties can be systematically examined because all parameters are obtained simultaneously at the individual cell level.

3D RI maps of individual RBCs. In order to obtain 3D RI tomograms of the individual RBCs, cDOT measures multiple 2D optical-field images of a sample with different angles of illumination; then, the 3D RI tomogram of the sample is reconstructed using the diffraction optical tomography algorithm³⁰. Typically, 500 holograms are recorded with various illumination angles spanning from -43° to 43° with an angular step of 0.17° in the sample plane (inside the medium). The total measurement time is less than 0.5 s.

Compared to existing techniques to measure 3D shapes of RBCs (e.g. confocal microscopy), the present method does not require the labeling of cell surface and the measurement can be performed in a short time. More importantly, the present technique provides the quantitative imaging capability; the RI information of RBC cytoplasm can be quantitatively translated into the information of Hb.

As shown in Fig. 2, the 3D RI tomograms of individual RBCs with four different pathophysiological conditions (see the Materials and Methods) were measured using cDOT: RBCs from a healthy individual, RBCs from a patient with IDA, reticulocytes from a patient with a high reticulocyte count, and RBCs from a patient diagnosed with HS. The images presented in Fig. 2 are rendered isosurfaces of the 3D RI tomograms from each group. The reconstructed morphologies exhibit good agreement with the known reference ranges⁵. The RI tomograms of RBCs from the healthy individual exhibited the characteristic biconcave shape. RBCs from the patient with IDA exhibited decreases in the cell volume, whereas those from the patient with high reticulocyte content display a significant increase in mean volume. The RBCs from the patient diagnosed with HS exhibit a spherocytosis shape.

Characterizations of individual RBCs from the healthy, IDA, reticulocyte, and HS patients. Using cDOT, the complete properties (i.e. morphological, chemical, and mechanical information) of individual RBCs under the different pathophysiological conditions (healthy, IDA, reticulocyte, and HS) were quantitatively investigated. The 3D RI maps provide the structural details of the cell such as the cell volume, cell surface area, and sphericity (Fig. 1B). Measuring the 3D RI maps also enables the determination of the biochemical information of the Hb protein in individual RBCs. Furthermore, the mechanical properties of individual RBCs can also be measured by probing their dynamic membrane fluctuations, which are obtained from the dynamic 2D topographic measurements.

In order to validate the performance of cDOT with regard to single cell profiling, the volume, surface area, sphericity, Hb content, Hb concentration, and membrane fluctuation of individual RBCs with different pathophysiological conditions were measured. As presented in Fig. 3, the morphological, chemical, and mechanical properties of individual RBCs were retrieved from 57, 34, 58, and 53 cells of healthy, IDA, reticulocyte, and HS patients, respectively. The RBCs of the healthy, IDA, reticulocyte, and HS groups were classified based on their morphologies and other hematologic tests by a pathologist. For the healthy RBCs, the mean values for the volume, Hb content, and concentration were 94.8 ± 11.4 fl, 32.2 ± 4.2 pg, and 34.1 ± 2.9 g/dl, respectively. These values agree very well with the relevant values of MCV, MCH, and MCHC measured using an automatic blood cell counter (XE-2100TM, Sysmex, Kobe, Japan). In addition, the mean values of the surface area (137.8 ± 13.3 μm^2), sphericity (0.731 ± 0.05), and membrane fluctuation (40.1 ± 3.9 nm) of the healthy RBCs were also in good agreement with the previous results^{23,32-35}.

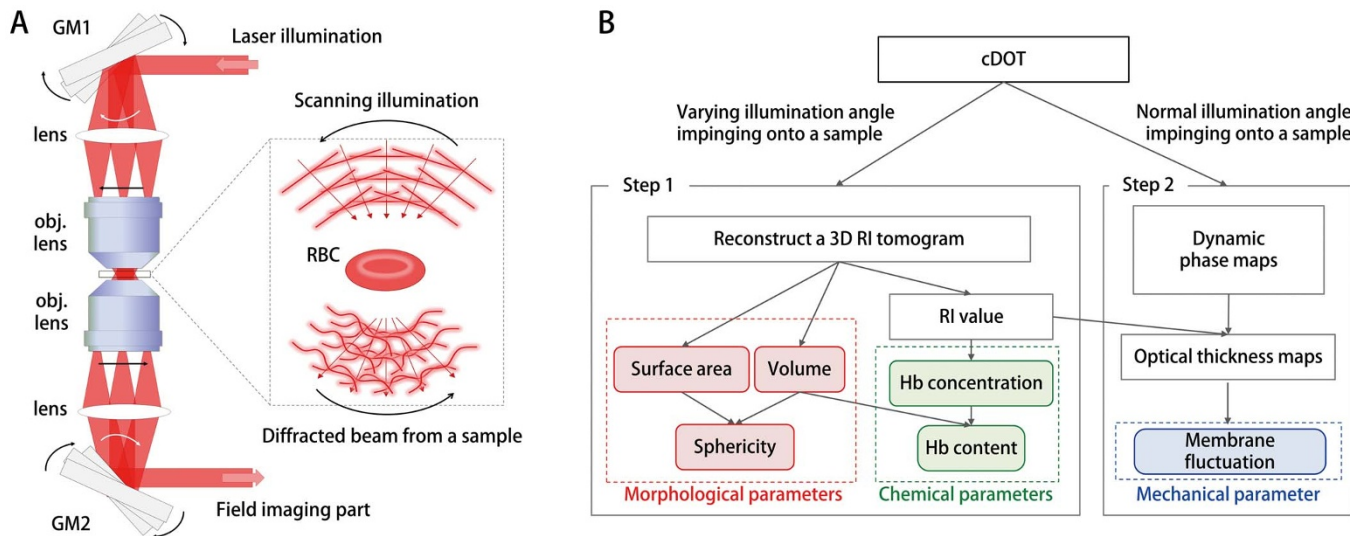


Figure 1 | Principle of cDOT and the analysis procedure for individual RBCs. (A) The cDOT setup is composed of two galvanometric mirrors (GM1, GM2) synchronized with each other and a field imaging part. A sample is positioned between two objective lenses. GM1-2: two-axis galvanometric mirrors. The angle of an illumination beam impinging onto the sample is scanned by rotating GM1 and is de-scanned by GM2 in a synchronized manner such that the angle of the beam reflected from GM2 remains unchanged. The sample is illuminated with a plane wave at different angles of illumination. (B) Schematic diagram of the analysis procedure for retrieving the red cell indices for individual RBCs using cDOT.

In general, patients with IDA exhibit decreased red cell values in MCV, MCH, and MCHC⁵. These trends were also exhibited in the measurements using cDOT and are consistent with previous studies^{36–38}. The mean values of the volume, Hb content, Hb concentration, surface area, sphericity, and membrane fluctuation of RBCs in the IDA patient were 59.7 ± 13.0 fl, 19.3 ± 4.8 pg, 32.2 ± 3.1 g/dl, $127.0 \pm 16.3 \mu\text{m}^2$, 0.582 ± 0.071 , and 37.9 ± 5.2 nm, respectively. The mean membrane fluctuation of the RBCs from the IDA patient was approximately 5% less than that of healthy RBCs, which indicates a decrease in cell deformability. In addition, compared with the healthy RBCs, the cell volume and sphericity of the IDA RBCs were significantly less, yet the surface area of the IDA RBCs was comparable with that of the healthy RBCs.

In patients with reticulocytes, the mean values of the volume, Hb content, Hb concentration, surface area, sphericity, and membrane fluctuation were 148.6 ± 29.1 fl, 39.1 ± 8.2 pg, 26.4 ± 2.5 g/dl, $220.4 \pm 31.6 \mu\text{m}^2$, 0.619 ± 0.076 , and 42.4 ± 4.2 nm, respectively. Compared with the reference range of the routinely used red cell indices in reticulocytes³⁹, relatively large values of the Hb content, surface area, and volume were measured using cDOT. It is considered that these results originate from the uniqueness of cDOT in terms of selectivity and sensitivity.

In the RBCs from the patient with HS, the mean values of the volume, Hb content, Hb concentration, surface area, sphericity, and membrane fluctuation were 73.3 ± 19.9 fl, 26.1 ± 5.5 pg, 36.6 ± 8.2 g/dl, $95.0 \pm 15.6 \mu\text{m}^2$, 0.888 ± 0.049 , and 36.6 ± 8.2 nm, respectively. The measured red cell indices, excluding

the membrane fluctuation, exhibit good agreement with the previous results^{40–45}.

It is noteworthy that the significantly decreased volume and Hb content of the IDA RBCs, the surface area and volume of the HS RBCs, and the increased volume, Hb content, and surface area of the reticulocytes, compared with healthy RBCs, presumably resulted from the selective and sensitive measurements that are enabled using cDOT. The values for sphericity clearly demonstrated that the HS RBCs had distinct spherical morphologies compared with those of the other groups.

2D correlation analyses between the morphological and chemical parameters. The ability of cDOT to measure the red cell indices of individual RBCs enables the possibility of correlation analyses because the indices are measured simultaneously at the individual cell level. Previously correlation analyses on red cell indices had been presented^{46,47}, but with only limited number of parameters.

Figure 4 presents the correlation analyses between the morphological and chemical parameters of the four groups. In particular, the overall correlation trends in the healthy RBCs and reticulocytes were consistent with the previous research finding of Higgins *et al.* (Fig. 4A)⁴⁸. While they reported impressive analyses of the correlation between the volume and Hb content in both RBCs and reticulocytes, the individual data were obtained from the CBC measurements of a sub-group of blood samples, not from individual cells. To date, the present work is the first reported demonstration of 2D correlation analyses of red cell indices on a cell-to-cell basis.

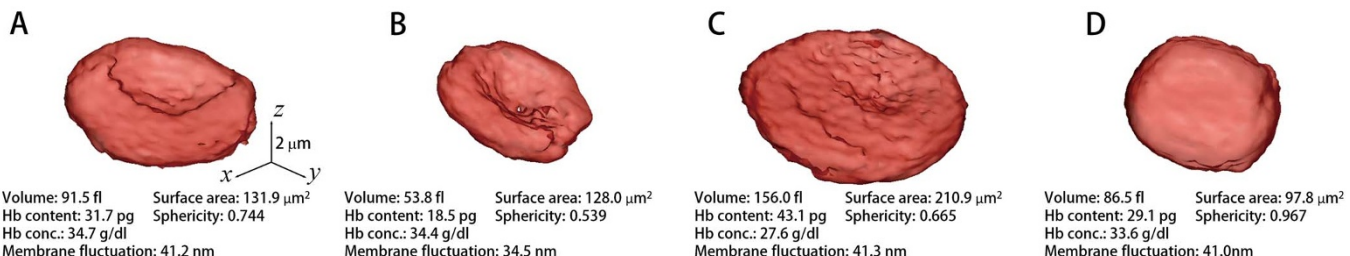


Figure 2 | 3D rendered isosurfaces of RI maps of individual RBCs from (A) healthy, (B) IDA, (C) reticulocyte, and (D) HS red blood cells (see also Supplementary Video 1 online).

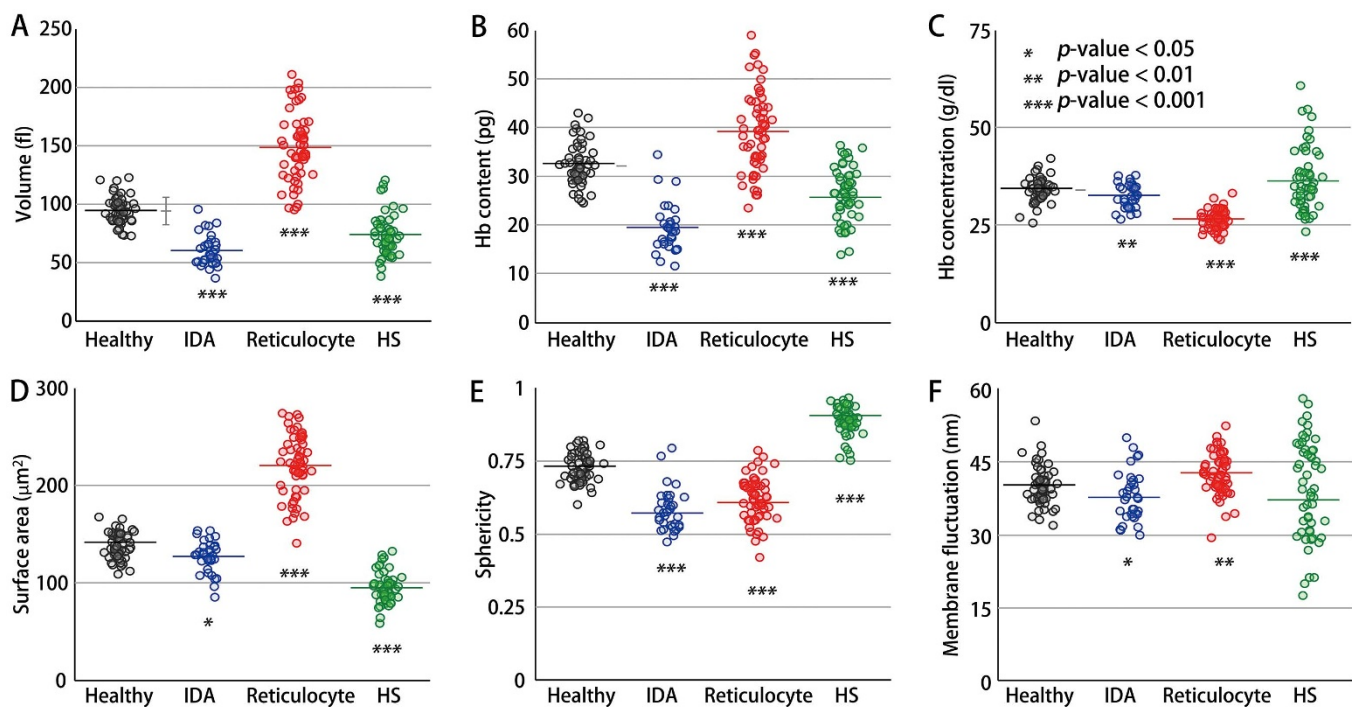


Figure 3 | Six red cell indices for healthy, IDA, reticulocyte, and HS red blood cells: (A) volume, (B) Hb content, (C) Hb concentration, (D) surface area, (E) sphericity, and (F) membrane fluctuation. The open circles correspond to individual RBC measurements. The horizontal lines in the open circles represent the mean values of each group. In the healthy RBCs, the gray horizontal lines correspond to the results of the relevant CBC measurement.

The correlations between the red cell indices enable understanding of the cellular physiology of RBCs in detail. For example, except for the HS RBCs, the Hb concentration for other groups is nearly constant and unchanged (Figs. 4A–B). The reticulocytes clearly exhibit a lower Hb concentration regardless of their volume. However, the HS RBCs exhibited a large polydispersity in the Hb concentration in the range of 20–60 g/dl. The correlation analyses between the cell volume and surface area (Fig. 4C), and between the Hb content and surface area (Fig. 4D), exhibited strong positive correlations for all groups. However, the ratios between the cell volumes and surface areas differed among all groups. In comparison with the healthy RBCs, the HS group exhibited an increase in the ratio, whereas the IDA group exhibited a slight decrease (the dotted lines in Fig. 4C). The surface area-to-volume ratios were 1.46 ± 0.12 , 2.18 ± 0.33 , 1.52 ± 0.26 , and 1.32 ± 0.13 for the RBCs in the healthy, IDA, reticulocytes, and HS patients, respectively. In particular, the ratio between the cell volumes and surface areas appeared to be common in the RBCs except the HS RBCs, which could be explained by the spherical shapes of the cells, as shown with the high values in sphericity (Figs. 4G–J). Interestingly, in all groups, individual RBCs with higher Hb concentrations exhibited lower values in their cell volumes and surface areas (Figs. 4B&E), which is consistent with the previous research undertaken for populated cells⁴⁹.

The correlations between the red cell indices also demonstrated that they could classify different pathophysiological conditions of RBCs, which enables opportunities to provide new methods of diagnosis. For example, the correlations between the cell volume and sphericity exhibit distinct variations between the groups (see the fitted Gaussian circles in Fig. 4H). Interestingly, the correlation between the surface area and sphericity exhibited similar trends for the groups of healthy RBCs, reticulocytes, and HS (the dotted line in Fig. 4G). Furthermore, as their surface areas decreased, the RBCs exhibited higher sphericity. However, the result demonstrated that the surface area of the RBCs in IDA was not related to sphericity; they exhibited diverse values in sphericity while maintaining a constant surface area, which could be explained by pathological findings of

IDA, ineffective hemoglobin production and decreased cell volume but unaffected cell membrane.

2D correlation analyses of the mechanical parameter versus the morphological and chemical parameters. In order to relate the mechanical properties of individual RBCs to the structural and biochemical properties, the correlations between the membrane fluctuations in RBCs with other red cell indices were analyzed (Fig. 5). The changes in the membrane fluctuations indicated alterations in the biomechanical properties of RBCs, including the shear modulus, bending modulus, and area expansion modulus of the cell membrane cortex, as well as the cytoplasmic viscosity^{3,23}. Previously, the membrane fluctuations and red cell indices have been measured for the various stages of malaria². However, these parameters have been measured separately using two different techniques; therefore, they have been investigated at the blood level, not at the individual cell level. Because cDOT measures the 3D RI maps and dynamic membrane fluctuations of individual RBCs simultaneously, their mechanical properties can be related to the structural and biochemical properties at the cellular level.

Figure 5 presents the correlation analyses of the mechanical parameters with the morphological and chemical parameters of the four groups. Interestingly, the membrane fluctuations in RBCs of all four groups exhibited strong negative correlations with the Hb concentration (Fig. 5A). The higher the Hb concentration, the less fluctuation the membranes had, which can be readily understood through the increased cytoplasmic viscosity that results from a high Hb concentration. In contrast to the healthy RBCs, the membrane fluctuation in the HS RBCs exhibited a large cell-to-cell variation, as well as relatively different trends in the correlations between the membrane fluctuation and cell volume, and between the membrane fluctuations and surface area (Figs. 5C–D). This large polydispersity observed in the correlation maps for the HS RBCs indicate a strong heterogeneity in the structures of the membrane cortex associated with diseases. The lower the cell volume or surface in the HS RBCs, the less membrane fluctuations were consistently observed

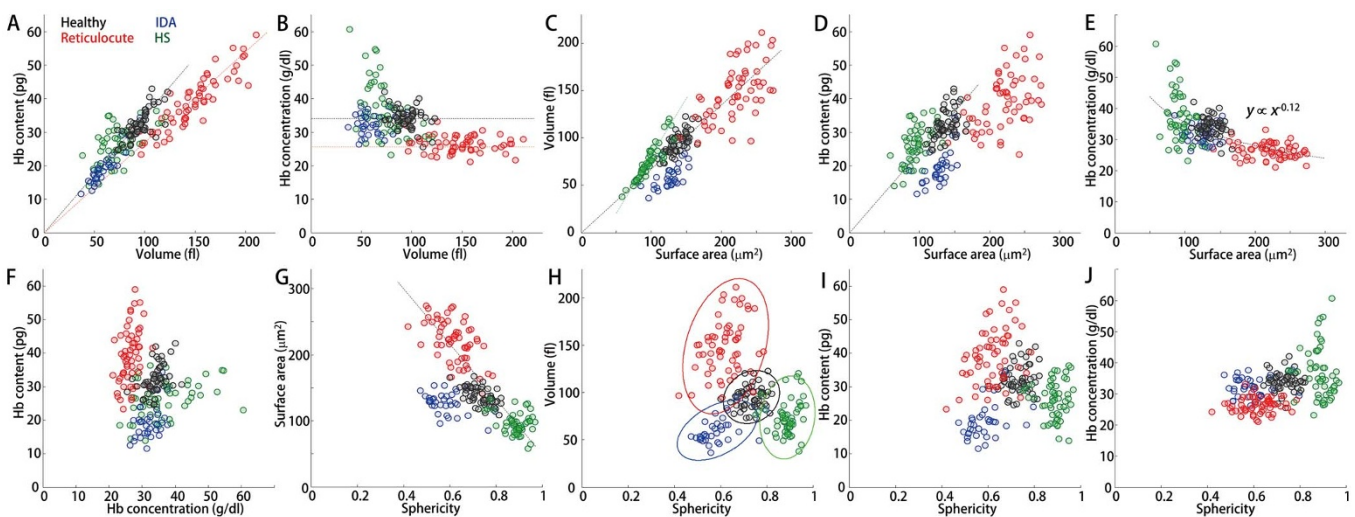


Figure 4 | Correlation maps between the morphological and chemical parameters for the healthy, IDA, reticulocyte, and HS red blood cells; correlation analyses between (A) volume and Hb content, (B) volume and Hb concentration, (C) surface area and volume, (D) surface area and Hb content, (E) surface area and Hb concentration, (F) Hb concentration and Hb content, (G) sphericity and surface area, (H) sphericity and volume, (I) sphericity and Hb content, and (J) sphericity and Hb concentration. The dotted lines are shown for guidance of linear relationships.

(Figs. 5C–D). This correlation analysis can support the previous studies that reported the reduced deformability in HS resulting from the loss of membrane surface area^{42,50,51}. Interestingly, the reticulocytes exhibited relatively constant membrane fluctuations regardless of the cell morphology [cell volume, surface area, and sphericity; red dotted lines in (Figs. 5B–D)].

The fluctuating amplitudes in the IDA RBCs exhibited comparable values as in the HS RBCs (Fig. 4F). However, the correlation analyses of the membrane fluctuations revealed that the IDA RBCs exhibited completely different tendencies in comparison with the HS RBCs. The membrane fluctuations of the IDA RBCs exhibited little correlation with the cell volume or surface area (Figs. 5C and 5D, respectively). This indicates that the origins of the reduced fluctuations would differ for the IDA and HS RBCs. The oxygen carrying capacity is primarily determined using the amount of Hb. However, the Hb amount and mechanical properties of individual RBCs also influence the oxygen carrying capacity because their deformability is crucial for RBCs to circulate. The reduced membrane deformability, which was manifested by the decreased dynamic membrane fluctuation, might explain the inefficient oxygen carrying capacity in IDA patients. Interestingly, the HS RBCs exhibited a narrow sphericity distribution despite the high cell-to-cell variation in the membrane fluctuations.

Conclusions. In this paper, employing cDOT, a precise and sensitive optical holographic technique, we performed the measurements of structural, chemical, and mechanical properties of individual human RBCs. The primary advantage of cDOT is its ability to analyze single

cell profiling for individual RBCs. cDOT can provide not only routine red cell indices but also additional indices such as sphericity, surface area, and membrane fluctuation. The retrieved structural, chemical, and mechanical information for RBCs can serve as important indicators for hemodiagnosis, and cDOT precisely measures these parameters at the individual cell level. Furthermore, secondary parameters such as RDW can also be directly obtained from these measurements. Importantly, the correlation analyses between the indices were performed at the single cell level, which can be further analyzed quantitatively for better understanding of the pathophysiological mechanism behind human diseases. For example, important mechanical properties of cell membrane cortex, which can be extracted by analyzing the dynamic membrane fluctuation in RBCs^{23,52–54}, may provide in-depth understanding of pathophysiology^{1,55} and ATP-dependent metabolic processes^{56–58} of RBCs together with simultaneously morphological and chemical properties of the cell at the individual cell level.

Although only four different RBC groups were examined, this method is readily applicable in other RBC-related diseases such as malaria^{59–61} and sickle cell diseases^{3,62,63}. In order for cDOT to be extrapolated to clinical applications, it requires high-throughput measurements. Currently, the measurement time for probing one cell is nearly 3 sec, but this time is not limited. Recently, our group has shown that the measurement and reconstruction speed for diffraction optical tomography can be significantly improved and done in real time, employing sparse illuminations and graphic processor unit (GPU) implementation¹⁹. Furthermore, the present approach can

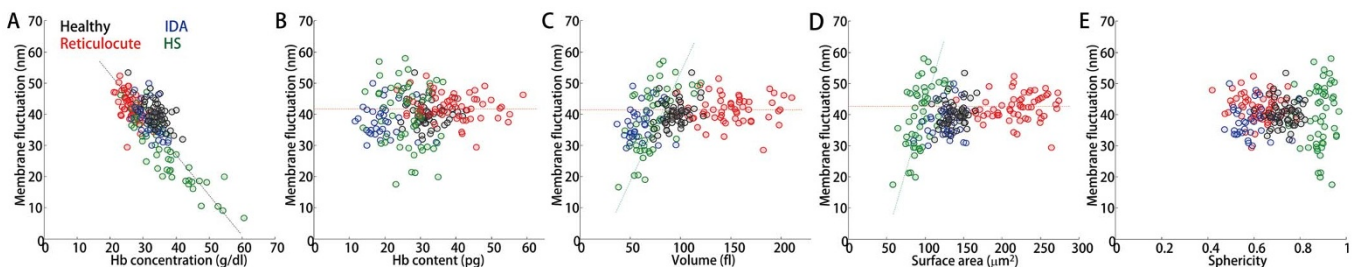


Figure 5 | Correlation maps of the mechanical parameter vs. the morphological and chemical parameters with for healthy, IDA, reticulocyte, and HS red blood cells. Correlation analyses of the membrane fluctuation versus the (a) Hb concentration, (b) Hb content, (c) volume, (d) surface area, and (e) sphericity.



also be further extended employing multimodality imaging. For example, hyperspectral quantitative phase imaging may provide molecular-specific information via optical dispersion^{64–67} and polarization sensitive imaging modality^{68,69} can be utilized for investigating optical dispersion properties in RBCs including sickle cell diseases^{3,63}. The instrumentation for the present approach can also be further simplified such that an existing optical microscope can be utilized by attaching a quantitative phase imaging unit⁷⁰, which may extend the applicability of the technique. Employing the principles of flow cytometry and optimizing the measurement instruments, the measurement speed can be further enhanced. Furthermore, cDOT can also be applied to other cell types including white blood cells⁷¹, circulating tumor cells, bacterial cells⁷², and endothelial cells for biophysical and medical purposes.

Methods

Sample preparation. Peripheral blood was drawn into EDTA treated anticoagulant tube via Vacutainer® (BD, Franklin Lakes, NJ, U.S.A.) and parameters of red blood cells (RBCs) were measured using an automated hematology analyzer (XE-2100, Sysmex, Kobe, Japan). Samples obtained from a healthy individual, a patient with iron deficiency anemia (IDA) with significantly decreased level of mean corpuscular volume (MCV), mean corpuscular hemoglobin concentration (MCHC), and hemoglobin (Hb) content, a patient with high level of reticulocytes, and a patient diagnosed with hereditary spherocytosis (HS) were stored in 4°C. For separation of reticulocytes, RBCs were first washed three times in saline by 900–1000 × g centrifugation for 5–15 minutes and supernatant fluid was removed without disturbing the buffy coat. 10–15 of microhematocrit tubes were filled with washed RBCs and centrifuged for 15 min at 2000 g and the top 5 mm of microhematocrit tubes were cut to obtain the least dense circulating red cells, namely reticulocytes. Red cell indices of the separated reticulocytes were measured with the automatic hematology analyzer. The methods were carried out in accordance with the approved guidelines. This study and all experimental protocol were approved by the ASAN Medical Center Institutional Review Board (IRB project number:#IRB-13-90) and the KAIST Institutional Review Board (IRB project number: 2012-0128). Blood samples were collected for regular course of patient care in Asan Medical Center, and we selected patients who had written the informed consent for using their archival tissues for genetic testing. All data was de-identified.

1. Suresh, S. Mechanical response of human red blood cells in health and disease: some structure-property-function relationships. *J. Mater. Res.* **21**, 1872 (2006).
2. Park, Y. *et al.* Refractive index maps and membrane dynamics of human red blood cells parasitized by Plasmodium falciparum. *Proc. Natl. Acad. Sci. USA* **105**, 13730–13735 (2008).
3. Byun, H. S. *et al.* Optical measurement of biomechanical properties of individual erythrocytes from a sickle cell patient. *Acta Biomater.* **8**, 4130–4138 (2012).
4. Mills, J. P. *et al.* Effect of plasmoidal RESA protein on deformability of human red blood cells harboring Plasmodium falciparum. *Proc. Natl. Acad. Sci. USA* **104**, 9213–9217 (2007).
5. Kaushansky, K. *Williams hematology*, (McGraw-Hill Medical New York, 2010).
6. Weatherall, D. J. Systems biology and red cells. *N. Engl. J. Med.* **364**, 376–377 (2011).
7. Hochmuth, R. M. Micropipette aspiration of living cells. *J Biomech* **33**, 15–22 (2000).
8. Sem'yanov, K. A., Tarasov, P. A., Soini, J. T., Petrov, A. K. & Maltsev, V. P. Calibration-free method to determine the size and hemoglobin concentration of individual red blood cells from light scattering. *Appl. Opt.* **39**, 5884–5889 (2000).
9. Dao, M., Lim, C. & Suresh, S. Mechanics of the human red blood cell deformed by optical tweezers. *J. Mech. Phys. Solid* **51**, 2259–2280 (2003).
10. Esposito, A. *et al.* FRET imaging of hemoglobin concentration in Plasmodium falciparum-infected red cells. *PLoS One* **3**, e3780 (2008).
11. Rusciano, G. Experimental analysis of Hb oxy-deoxy transition in single optically stretched red blood cells. *Phys. Medica* **26**, 233–239 (2010).
12. DeBlois, R. & Bean, C. Counting and sizing of submicron particles by the resistive pulse technique. *Rev. Sci. Instrum.* **41**, 909–916 (1970).
13. Mohandas, N. *et al.* Accurate and independent measurement of volume and hemoglobin concentration of individual red cells by laser light scattering. *Blood* **68**, 506–513 (1986).
14. Tomaiuolo, G., Rossi, D., Caserta, S., Cesarelli, M. & Guido, S. Comparison of two flow-based imaging methods to measure individual red blood cell area and volume. *Cytometry. Part A : the journal of the International Society for Analytical Cytology* **81**, 1040–1047 (2012).
15. Waugh, R. E. *et al.* Rheologic Properties of Senescent Erythrocytes - Loss of Surface-Area and Volume with Red-Blood-Cell Age. *Blood* **79**, 1351–1358 (1992).
16. Popescu, G. *Quantitative Phase Imaging of Cells and Tissues*, (McGraw-Hill Professional, 2011).
17. Lee, K. *et al.* Quantitative phase imaging techniques for the study of cell pathophysiology: from principles to applications. *Sensors* **13**, 4170–4191 (2013).
18. Popescu, G. *et al.* Imaging red blood cell dynamics by quantitative phase microscopy. *Blood Cells Mol. Dis.* **41**, 10–16 (2008).
19. Kim, K., Kim, K. S., Park, H., Ye, J. C. & Park, Y. Real-time visualization of 3-D dynamic microscopic objects using optical diffraction tomography. *Opt Express* **21**, 32269–32278 (2013).
20. Popescu, G. *et al.* Optical imaging of cell mass and growth dynamics. *Am J Physiol Cell Physiol* **295**, C538–544 (2008).
21. Kemper, B. & von Bally, G. Digital holographic microscopy for live cell applications and technical inspection. *Appl. Opt.* **47**, A52–A61 (2008).
22. Rappaz, B. *et al.* Comparative study of human erythrocytes by digital holographic microscopy, confocal microscopy, and impedance volume analyzer. *Cytometry. Part A : the journal of the International Society for Analytical Cytology* **73**, 895–903 (2008).
23. Park, Y. K. *et al.* Measurement of red blood cell mechanics during morphological changes. *Proc. Natl. Acad. Sci. USA* **107**, 6731 (2010).
24. Popescu, G., Park, Y. K., Dasari, R. R., Badizadegan, K. & Feld, M. S. Coherence properties of red blood cell membrane motions. *Phys Rev E* **76**, 31902 (2007).
25. Rappaz, B. *et al.* Spatial analysis of erythrocyte membrane fluctuations by digital holographic microscopy. *Blood Cells Mol. Dis.* **42**, 228–232 (2009).
26. Kim, Y. *et al.* Common-path diffraction optical tomography for investigation of three-dimensional structures and dynamics of biological cells. *Opt Express* **22**, 10398–10407 (2014).
27. Debnath, S. K. & Park, Y. Real-time quantitative phase imaging with a spatial phase-shifting algorithm. *Opt Lett* **36**, 4677–4679 (2011).
28. Popescu, G., Ikeda, T., Dasari, R. R. & Feld, M. S. Diffraction phase microscopy for quantifying cell structure and dynamics. *Opt. Lett.* **31**, 775–777 (2006).
29. Park, Y., Popescu, G., Badizadegan, K., Dasari, R. R. & Feld, M. S. Diffraction phase and fluorescence microscopy. *Opt Express* **14**, 8263–8268 (2006).
30. Kim, K. *et al.* High-resolution three-dimensional imaging of red blood cells parasitized by Plasmodium falciparum and in situ hemozoin crystals using optical diffraction tomography. *J. Biomed. Opt.* **19**, 011005 (2013).
31. Wolf, E. Three-dimensional structure determination of semi-transparent objects from holographic data. *Opt Commun* **1**, 4 (1969).
32. Pham, H. V., Bhaduri, B., Tangella, K., Best-Popescu, C. & Popescu, G. Real time blood testing using quantitative phase imaging. *PLoS One* **8**, e55676 (2013).
33. Clark, M. R., Mohandas, N. & Shohet, S. B. Osmotic gradient ektacytometry: comprehensive characterization of red cell volume and surface maintenance. *Blood* **61**, 899–910 (1983).
34. Canham, P. & Burton, A. C. Distribution of size and shape in populations of normal human red cells. *Circ Res* **22**, 405–422 (1968).
35. Canham, P. B. The minimum energy of bending as a possible explanation of the biconcave shape of the human red blood cell*. *J. Therm. Biol.* **26**, 61–81 (1970).
36. Yip, R. *et al.* Red cell membrane stiffness in iron deficiency. *Blood* **62**, 99–106 (1983).
37. Ntaios, G. *et al.* Discrimination indices as screening tests for β-thalassemic trait. *Ann. Hematol.* **86**, 487–491 (2007).
38. Brandão, M. M. *et al.* Impaired red cell deformability in iron deficient subjects. *Clin. Hemorheol. Microcirc.* **43**, 217–221 (2009).
39. d'Onofrio, G. *et al.* Simultaneous measurement of reticulocyte and red blood cell indices in healthy subjects and patients with microcytic and macrocytic anemia. *Blood* **85**, 818–823 (1995).
40. Da Costa, L., Galimand, J., Fenneteau, O. & Mohandas, N. Hereditary spherocytosis, elliptocytosis, and other red cell membrane disorders. *Blood Rev* **27**, 167–178 (2013).
41. Cynober, T., Mohandas, N. & Tchernia, G. Red cell abnormalities in hereditary spherocytosis: relevance to diagnosis and understanding of the variable expression of clinical severity. *J. Lab. Clin. Med.* **128**, 259–269 (1996).
42. Da Costa, L. *et al.* Temporal differences in membrane loss lead to distinct reticulocyte features in hereditary spherocytosis and in immune hemolytic anemia. *Blood* **98**, 2894–2899 (2001).
43. Chasis, J., Agre, P. & Mohandas, N. Decreased membrane mechanical stability and in vivo loss of surface area reflect spectrin deficiencies in hereditary spherocytosis. *J. Clin. Invest.* **82**, 617 (1988).
44. Waugh, R. E. & Agre, P. Reductions of erythrocyte membrane viscoelastic coefficients reflect spectrin deficiencies in hereditary spherocytosis. *J. Clin. Invest.* **81**, 133 (1988).
45. Bolton-Maggs, P. *et al.* Guidelines for the diagnosis and management of hereditary spherocytosis. *Brit J Haematol* **126**, 455–474 (2004).
46. Tycko, D., Metz, M., Epstein, E. & Grinbaum, A. Flow-cytometric light scattering measurement of red blood cell volume and hemoglobin concentration. *Applied optics* **24**, 1355–1365 (1985).
47. Schonbrun, E., Malka, R., Caprio, G., Schaak, D. & Higgins, J. M. Quantitative absorption cytometry for measuring red blood cell hemoglobin mass and volume. *Cytometry Part A* **85**, 338 (2014).
48. Higgins, J. M. & Mahadevan, L. Physiological and pathological population dynamics of circulating human red blood cells. *Proc. Natl. Acad. Sci. USA* **107**, 20587–20592 (2010).
49. Waugh, R. E. *et al.* Rheologic properties of senescent erythrocytes: loss of surface area and volume with red blood cell age. *Blood* **79**, 1351–1358 (1992).
50. Nakashima, K. & Beutler, E. Erythrocyte cellular and membrane deformability in hereditary spherocytosis. *Blood* **53**, 481–485 (1979).



51. Perrotta, S., Gallagher, P. G. & Mohandas, N. Hereditary spherocytosis. *Lancet* **372**, 1411–1426 (2008).
52. Park, Y. K., Best, C. A. & Popescu, G. Optical sensing of red blood cell dynamics. In *Mechanobiology of Cell-cell and Cell-matrix Interactions* 279 (Springer, 2011).
53. Kim, Y., Kim, K. & Park, Y. Measurement Techniques for Red Blood Cell Deformability: Recent Advances. In *Blood Cell - An Overview of Studies in Hematology* (ed. Moschandreas, T.E.) 167–194 (INTECH, 2012).
54. Park, Y. *et al.* Measurement of the nonlinear elasticity of red blood cell membranes. *Phys Rev E* **83**(2011).
55. Diez-Silva, M., Dao, M., Han, J., Lim, C. T. & Suresh, S. Shape and biomechanical characteristics of human red blood cells in health and disease. *MRS bulletin* **35**, 382–388 (2010).
56. Park, Y. K. *et al.* Metabolic remodeling of the human red blood cell membrane. *Proc. Natl. Acad. Sci. USA* **107**, 1289 (2010).
57. Boss, D. *et al.* Spatially-resolved eigenmode decomposition of red blood cells membrane fluctuations questions the role of ATP in flickering. *PLoS One* **7**, e40667 (2012).
58. Betz, T., Lenz, M., Joanny, J. & Sykes, C. ATP-dependent mechanics of red blood cells. *Proc. Natl. Acad. Sci. USA* **106**, 15312–15317 (2009).
59. Chandramohanadas, R. *et al.* Biophysics of malarial parasite exit from infected erythrocytes. *PLoS One* **6**, e20869 (2011).
60. Diez-Silva, M. *et al.* Pf155/RESA protein influences the dynamic microcirculatory behavior of ring-stage Plasmodium falciparum infected red blood cells. *Sci. Rep.* (2012).
61. Park, Y. *et al.* Static and dynamic light scattering of healthy and malaria-parasite invaded red blood cells. *J. Biomed. Opt.* **15**, 020506 (2010).
62. Shaked, N. T., Satter32white, L. L., Telen, M. J., Truskey, G. A. & Wax, A. Quantitative microscopy and nanoscopy of sickle red blood cells performed by wide field digital interferometry. *J. Biomed. Opt.* **16**, 030506–030506–030503 (2011).
63. Kim, Y., Higgins, J. M., Dasari, R. R., Suresh, S. & Park, Y. K. Anisotropic light scattering of individual sickle red blood cells. *J. Biomed. Opt.* **17**, 040501–040501 (2012).
64. Jang, Y., Jang, J. & Park, Y. Dynamic spectroscopic phase microscopy for quantifying hemoglobin concentration and dynamic membrane fluctuation in red blood cells. *Opt Express* **20** (2012).
65. Jung, J. & Park, Y. Spectro-angular light scattering measurements of individual microscopic objects. *Opt Express* **22**, 4108–4114 (2014).
66. Jung, J., Jang, J. & Park, Y. Spectro-refractometry of individual microscopic objects using swept-source quantitative phase imaging. *Anal. Chem.* (2013).
67. Park, Y., Yamauchi, T., Choi, W., Dasari, R. & Feld, M. S. Spectroscopic phase microscopy for quantifying hemoglobin concentrations in intact red blood cells. *Opt. Lett.* **34**, 3668–3670 (2009).
68. Wang, Z., Millet, L. J., Gillette, M. U. & Popescu, G. Jones phase microscopy of transparent and anisotropic samples. *Opt. Lett.* **33**, 1270–1272 (2008).
69. Kim, Y., Jeong, J., Jang, J., Kim, M. W. & Park, Y. Polarization holographic microscopy for extracting spatio-temporally resolved Jones matrix. *Opt Express* **20** (2012).
70. Lee, K. & Park, Y. Quantitative phase imaging unit. *Opt Lett* **39**, 3630–3633 (2014).
71. Garay, J. *et al.* Crosstalk between PKA and Epac regulates the phenotypic maturation and function of human dendritic cells. *J Immunol* **185**, 3227–3238 (2010).
72. Jo, Y. *et al.* Angle-resolved light scattering of individual rod-shaped bacteria based on Fourier transform light scattering. *Sci. Rep.* **4** (2014).

Acknowledgments

The authors thank K.R. Lee for helpful discussions. This work was supported by KAIST, National Research Foundation (NRF) of Korea (2012R1A1A1009082, 2013K1A3A1A09076135, M3C1A1-048860, 2013M3C1A3063046, NRF-2012-M3C1A1-048860, 2013R1A1A3011886, 2014M3C1A3052537), and KUSTAR-KAIST project, is supported by Global Ph.D. Fellowship from NRF.

Author contribution

Y.K and Y.P. developed the experimental setup. Y.K., H.S., and H.P. performed the experiments and analyzed the data. H.S. performed the sample preparation. K.K. established the reconstruction algorithm for the diffraction optical tomography. S.J. and Y.P. conceived and supervised the study. All authors discussed the experimental results and wrote the manuscript.

Additional information

Supplementary Information accompanies this paper at <http://www.nature.com/scientificreports/>

Competing financial interests: The authors declare no competing financial interests.

How to cite this article: Kim, Y. *et al.* Profiling individual human red blood cells using common-path diffraction optical tomography. *Sci. Rep.* **4**, 6659; DOI:10.1038/srep06659 (2014).

This work is licensed under a Creative Commons Attribution-NonCommercial-ShareAlike 4.0 International License. The images or other third party material in this article are included in the article's Creative Commons license, unless indicated otherwise in the credit line; if the material is not included under the Creative Commons license, users will need to obtain permission from the license holder in order to reproduce the material. To view a copy of this license, visit <http://creativecommons.org/licenses/by-nc-sa/4.0/>